Physica C 185-189 (1991) 147-155
North-Holland

PHYSICA C

ELECTRONS, PHONONS, AND THEIR INTERACTION IN $YBa_2Cu_3O_7$

O.K. ANDERSEN, A.I. LIECHTENSTEIN, O. RODRIGUEZ, I.I. MAZIN,
O. JEPSEN, V.P. ANTROPOV, O. GUNNARSSON, and S. GOPALAN

Max–Planck Institut für Festkörperforschung, D–7000 Stuttgart 80, FRG.

We have performed LDA calculations of structure, phonon frequencies, and the electron-phonon interaction. We find good agreement with available data and estimate: λ=1. Saddlepoints 20 meV below the Fermi level are important.

INTRODUCTION

For the high-temperature copper-oxide superconductors experimental evidence is mounting[1] that the electronic structure in the normal, metallic state is Fermi-liquid like, and that the electron-phonon (e–ph) interaction is not weak.[2] [3] Despite the smallness of the isotope effect, this conventional mechanism for superconductivity might therefore play a role.

The Fermi surfaces resemble those predicted by *ab initio* band-structure calculations[4] using the local-density approximation (LDA). Moreover, for $YBa_2Cu_3O_7$ (1237), the structurally best characterized high-temperature superconductor, the LDA band structure reproduces not only the optical spectra in the 1–10eV region[5] but also the resonant Raman spectra for scattering off the five optical phonons with Γ_1 symmetry (phonon-modulation of the dielectric function).[6]

For 1237, we[7] and independently Cohen, Pickett, and Krakauer[8] have tried to assess the strength of the e–ph coupling (λ) *ab initio*, by performing LDA calculations of phonon frequencies and eigenvectors, of the band structure, and of the e–ph interaction. For the electrons we use the LDA-bands. Our frozen-phonon supercell calculations can only be performed for wave-vectors (**q**) at high-symmetry points and for a few of the 39 phonon-modes (ν) so that a proper sampling over all phonons is not possible. The resulting $\lambda \equiv \Sigma\lambda_{\nu\mathbf{q}} \approx 1$ is therefore only accurate numerically to within a factor of about two but, nevertheless, it indicates that the e–ph coupling is of intermediate strength and too small to be the *sole* cause for superconductivity with T_C=92K, unless the LDA bands ought to be renormalized due to e–e interaction Our results for individual phonons are numerically more precise and may be checked with experiments in detail. This has, most notably, been done for the Raman-active plane-oxygen and apical-oxygen modes observed to broaden and to soften, or harden, upon cooling below T_c. These effects reflect the strength of $\lambda^s_{\nu\mathbf{q}}$ in the superconducting state (^{s}).

In this paper, we shall review our results for **q**= (0,0,0)≡Γ and present new results for **q**=$(\pi/a,\pi/b,0)\equiv$ S and **q**=$(0,\pi/b,0)\equiv$Y. The latter will be compared with phonons measured by neutron-scattering.[9] Moreover, we shall compare our Fermi surface with dHvA measurements, and present details of the energy bands and their adiabatic phonon-deformation. Finally, we shall calculate *Im* $\chi^0(\mathbf{q},\omega)$ in the constant-matrix-element approximation for **q** throughout the Brillouin zone. It turns out that saddlepoints in the CuO_2 plane-band, merely 20meV below the Fermi level, give rise to nesting-anomalies near **q** ≈ $^2/_3\Gamma$Y and $^1/_2\Gamma$X. These may be the origin of observed phonon smearings[9] and dynamical superstructures.[3] If the saddlepoints are really that close to ϵ_f, this might explain why the quasi-electron linewidths are observed[10] to increase faster than $(\epsilon-\epsilon_f)^2$. On the other hand, it would seem to invalidate the use of conventional Eliashberg theory, and even Migdals theorem, because the gap, the phononic, and the electronic energy scales are now the same.

2 METHOD

For the LDA calculations we used Methfessels full-potential LMTO version,[11] which is the most accurate and efficient technique presently available. The multiple-κ basis set and the MT–radii were carefully chosen. The relative sub-band positions were converged to better than 5meV. Such high accuracy is needed in order to treat the e–ph interaction properly numerically and, for the same reason, we found it necessary to perform the self-consistent calculations with over 100 inequivalent k–points and the full–zone tetrahedron method. The Fermi–surface and line–integrals for the e–ph coupling employed LMTO bands calculated at a mesh of over 800 inequivalent k–points.

The phonon eigenvectors $e_{ij,\nu q}$ and frequencies squared $\omega^2_{\nu q}$ were obtained by diagonalization of the adiabatic dynamical matrix

$$D^{q}_{ij,i'j'} \equiv [M_j M_{j'}]^{\frac{1}{2}} \, \partial^2 E / \partial R^{q}_{ij} \partial R^{q}_{i'j'} \qquad (1)$$

for a given q and irreducible representation (we only considered the identity representation). M_j is the mass and ∂R^{0}_{ij} is the displacement in the i–direction of the j'th atom in the primitive cell. Using the q–supercell, the LDA total energy E was calculated as a function of the degrees of freedom (5 for Γ and S, and 7 for Y) for a large number of atomic displacements ($|\partial R^{0}_{ij}| = 0.04$—$0.08$Å) and least-squares fitted to a second– or third-order polynomium .

3 STRUCTURE AND PHONONS

From Table I we see that the calculated cell volume is 6% smaller than the volume measured at 300K (5% smaller than measured[12] at 103K). This overbinding is due to the LDA and is the largest structural error that we encounter. For all further calculations we decided to fix the volume at the experimental value although this usually causes the calculated phonon frequencies to be up to 10% too low. Also, we used the experimental a and b lattice constants.

For q=Γ the five modes which transform according to the identity representation displace apical oxygen (O4), barium, plane copper (Cu2), and plane oxygen (O2 and O3) in the z–direction and are even with respect to the Y inversion center. The calculated equilibrium positions are in excellent agreement with the experimental values (Table I). Even the socalled dimple, the vertical displacement of O2 and O3 out of the Cu2 planes towards Y, is accurately accounted for. The experimental dimple is slightly smaller for O2 than for O3, which lies above chain oxygen (O1). The chains run in the y–direction.

TABLE I. Static structural parameters.

	V(Å^3)	c/a	z/c_{exp}						(c_{exp}=11.68Å)	
			Cu1	O1	O4	Ba	Cu2	O2	O3	Y
Exp[13]	173.5	3.05	0	0	.158	.184	.356	.377	.379	.5
LDA	163.1	3.02			.157	.184	.355	.375	.375	

The phonon frequencies measured accurately by Raman scattering agree well with the ones calculated. This may bee seen from Table II, which also gives the calculated phonon eigenvectors. These form a unitary matrix which determines the displacement pattern for the νq–phonon as:

$$\delta R^{0}_{ij} = e_{ij,\nu q} [2 M_j \omega_{\nu q}]^{-\frac{1}{2}} \delta Q_{\nu q}. \qquad (2)$$

Analysis of the polarization dependence of the Raman intensities[6] confirm the theoretical eigenvectors, except for the strong mixing of the Ba and Cu2 modes caused by a (calculated) near degeneracy of the two pure modes. The observed Raman intensAy of the 54meV (440cm^{-1}) mode in z–polarization of the incomming and scattered light is solely due to the by–mixing of O4-character to the in-phase dimpling mode (O3+O2).[6] In the calculations, the latter mode showed the largest anharmonicity. We shall return to Table II when discussing the e–ph interaction in Sect. 5.

TABLE II. Γ_1–phonons: Frequencies, e-ph coupling constants in the superconducting state, and eigenvectors.

ω(meV)[a]		λ^s(%)		e				
Exp[2]	LDA	Exp	LDA	Ba_z	$Cu2_z$	$O3_z$–$O2_z$	$O3_z$+$O2_z$	$O4_z$
14	12		3.4	.65	.75	.05	–.07	–.07
19	16		0.7	.76	–.65	–.02	–.02	.04
41	41	2[14]	2.1	.01	.02	–.89	.43	.14
54	49	1[14]	1.0	.02	.04	–.44	–.76	–.47
62	57	1[15]	0.9	.03	.11	–.10	–.48	.87

[a] 1mRy ≈ 110cm^{-1} ≈ 13.6meV ≈ 160K ≈ 3.29THz.

Of the S_1-phonons, shown in Table III, the $Cu2_z$ and the plane-quadrupolar modes are calculated to have the lowest frequencies and smallest mixing. Our 44meV phonon is essentially a chain-quadrupolar ($O1_y$–$O4_z$) mode and we associate it with the 42meV phonon seen by neutron scattering to have strong transverse ($_z$) polarization.[9] The 50meV mode is plane-breathing with O4 moving inwards, towards Cu2, and O1 moving in-phase with O3. Finally, the 74meV mode is breathing of the entire O2–O3–O4 octahedron. The latter modes have been identified with neutron scattering and the agreement for the frequencies is excellent.

For the Y_Γ-phonons the identification of the experimental modes is less clear and the frequencies quoted in Table IV are merely the ones closest to our calculated values.

TABLE III. S_Γ-phonons: Frequencies, relative phonon line-widths, e-ph coupling constants, and eigenvectors.

ω(meV)		γ/ω(%)		$39\times\lambda$		e				
Exp[9]	LDA	LDA	pure	LDA	pure	$Cu2_z$	Qu.	$O1_y$	$O4_z$	Br.
	12	0.6	0.5	2.8	1.9	.99	.03	−.01	.11	−.01
	43	0.2	0.1	0.2	0.1	.03	−.97	.22	.03	.06
42	44	0.4	0.1	0.4	0.1	.07	.15	.77	−.60	−.14
54	50	1.3	0.4	1.4	0.4	.06	−.17	−.54	−.60	−.57
75	74	0.7	1.5	0.5	1.2	.06	−.02	−.26	−.52	.81

Quadrupolar ≡ $O3_y$–$O2_x$. Breathing ≡ $O3_y$+$O2_x$.

TABLE IV. Y_Γ-phonons: Frequencies, relative phonon line-widths, e-ph coupling constants, and eigenvectors.

ω(meV)		γ/ω	39λ	e						
Exp[9]	LDA	LDA pure	LDA pure	$Cu2_z$	Ba_y	Y_y	$O3_y$	$O2_z$	$O1_y$	$O4_z$
11	7	0.1	0.2	.82	.37	.25	.03	.33	.05	.13
18	16	1.2	3.3	.44	−.88	−.02	.18	−.07	−.02	−.08
28	26	0.1	0.1	.24	.12	−.91	−.04	−.12	.27	.11
43	37	0.2	0.2	.11	.26	.06	.64	−.48	.05	−.52
49	48	0.2	0.3	.27	.07	.08	−.62	−.64	−.33	−.11
59	56	0.2	0.2	.02	.06	−.30	.19	.26	−.89	−.09
61	64	0.2	0.2	.01	−.03	−.09	−.36	.40	.15	−.82

4 ELECTRONS

In Fig. 1 we show the LDA energy bands $\epsilon_{n\mathbf{k}}$ with the Fermi level ϵ_f being the energy zero. We clearly see the dispersive O4(z)-Cu1(y^2–z^2)-O1(y)-like antibonding "$pd\sigma$" chain band and the two O3(y)-Cu2(x^2–y^2)-O2(x)-like antibonding "$pd\sigma$" plane bands. A fourth band of O4(y)-character just crosses ϵ_f near the SR–line and

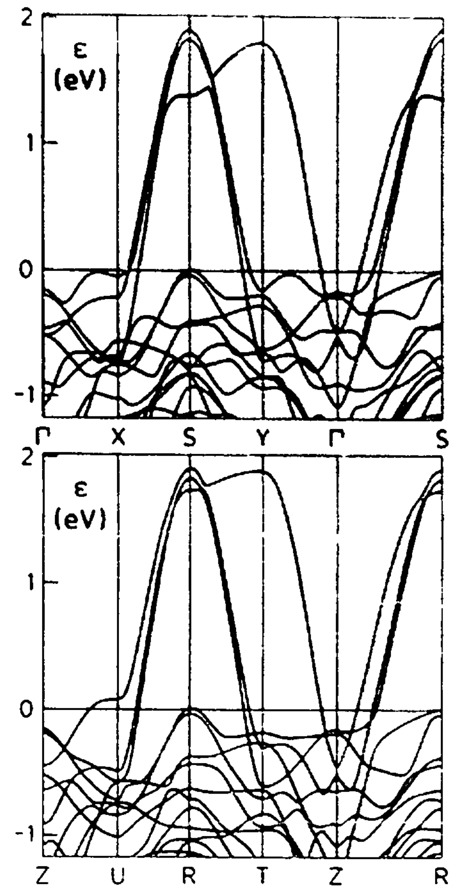

FIG. 1. Energy bands for k_z=0 (top) and π/c (bottom).

gives rise to a cylindrical hole-pocket, the "stick". The intersection of the Fermi surface (FS) with the k_z=0 and $k_z=\pi/c$-planes is shown in the upper part of Fig. 2. The irreducible part of the Brillouin zone has the shape of a flat square box and its intersections with the FS and with the ±20meV energy surfaces are shown in the lower part of Fig. 2.

This LDA FS is in surprisingly good agreement with the one obtained by angle-resolved photoemission considering the missing k_z- and limited ϵ-resolution of the experiment and the twinning of the crystal.[1] Moreover, the extremal areas of 0.014 and 0.021a_0^{-2} recently observed in a dHvA-experiment with a 100T pulsed field in the z-direction[16] agree well with our spin-split LDA extremal areas of 0.013 and 0.020a_0^{-2} for the stick. The cyclotron masses are 7.0 and 7.2m_0 and, compared with our LDA masses of 2.5 and 3.0m_0, we obtain mass

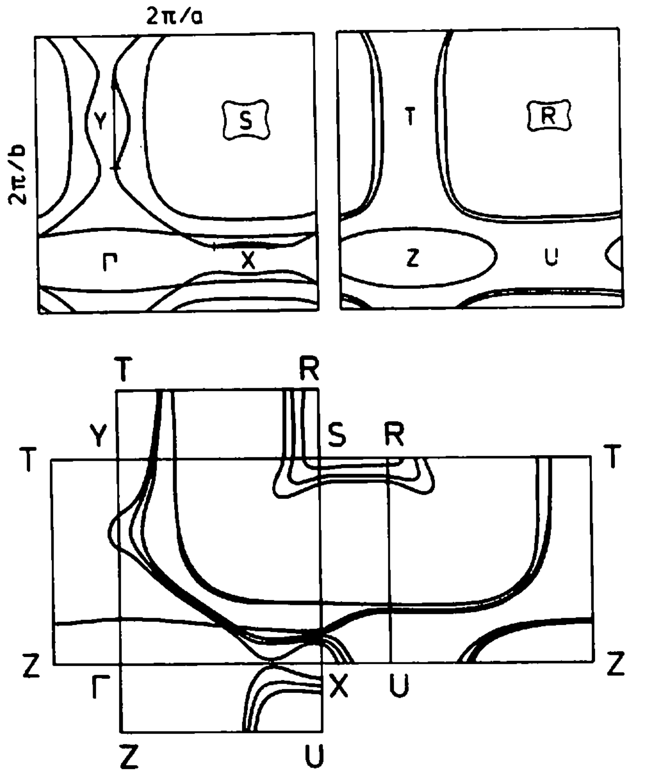

FIG. 2. Intersection of the FS with the planes k_z=0 (top left) and $k_z=\pi/c$ (top right). The arrows show the knuckle-knuckle nesting–vectors ($^2/_3\Gamma Y$ and $^1/_2\Gamma X$). Bottom: Intersection of the FS ϵ=0 and of the constant-energy surfaces ϵ=±20meV with the boundaries of the irreducible Brillouin-zone. The distance between constant-energy contours is inversely proportional to the Fermi velocity.

enhancements of 2.8 and 2.4.

We now discuss the bands and the FS. In a nearest-neighbor tight-binding model, the chain band would only disperse in the k_y-direction and would have its maximum in the **YSRT** plane and its minimum in the **ΓXUZ** plane; the FS would be an electron-wall centered around the **ΓXUZ**-plane. The two plane bands would be degenerate and disperse only in the k_x and k_y-directions with maximum at **SR**, saddlepoints at **XU** and **YT**, and minimum at **ΓZ**. For half filling, the Fermi level would be at the saddle-points and the plane FS would be a square column with faces **XYTU** and, hence, perfectly nesting with q=**S**.

Compared herewith the plane-sheets of the LDA Fermi surface for 1237 are two **SR**-centered hole-columns whose cross-sections with the $k_z=\pi/c$ plane are rounded squares with (100)-orientation. The reasons for this 45° turn are that O2-O3 hopping lifts the bands near the **ΓSRZ**-plane, that hybridization with the O4(z), Cu2(s), and Cu2($3z^2$–1) orbitals lifts the bands near the **XU** and the **YT** lines, and that the chain sheet hybridizes with the outer hole-column for $k_z=\pi/c$ and with the inner for k_z=0. The cross-sections of the hole-columns with the k_z=0 plane is similar for the inner column, but radically different for the outer column which is twisted to a (110)-orientation and has developed "knuckles" around the **X** and **Y** points. From the lower parts of Figs. 1 and 2 we see that the band becomes flat at the knuckles due to the presence of saddlepoints 15 and 25meV below ϵ_f. These are the tight-binding **X** and **Y** saddlepoints which have bifurcated to the positions **X**±$^1/_4$**ΓX** and **Y**±$^1/_3$**ΓY**. From the upper part of Fig. 2 one realizes that the inner, straight column is about half full and that the outer, twisted and knuckled column contains essentially all the holes doped by the chains. Of the two plane bands (Fig. 1) the upper band, giving rise to the twisted and knuckled column, is odd and the lower band, giving rise to the dull column, is even with respect to the yttrium mirror plane. We shall refer to these two bands as respectively the a– and the b-bands because the former is anti-bonding and the latter is bonding between the neighboring CuO_2 planes. The a–b splitting is seen to increase from about 0.1eV near the **ΓSRZ**-plane to about 0.5eV near **XU** and **YT**. This is mainly due to the presence of Cu2(s) character which couples the planes. Superposed on this effect is the hybridization with the chain band. Since the latter is even with respect to the mirror plane containing the chains it only hybridizes with the b-band for k_z=0 and only with the a–band for $k_z=\pi/c$. Near the knuckles of the a-band there is no hybridization with the chain.

The question arises: Why are, as seen in the upper part of Fig. 1, the a-band saddlepoints near ϵ_f (which are not chain-hybridized) shifted away from **X** and **Y** towards **Γ**? Fig. 3 shows the wavefunctions at **Y** and at $\frac{1}{3}$**ΓY**, near the saddlepoint. At both points there is substantial by-mixing of Cu2(s), Cu($3z^2$–1), and O4(z) character, but away from **Y** the by-mixing of O3(z) and

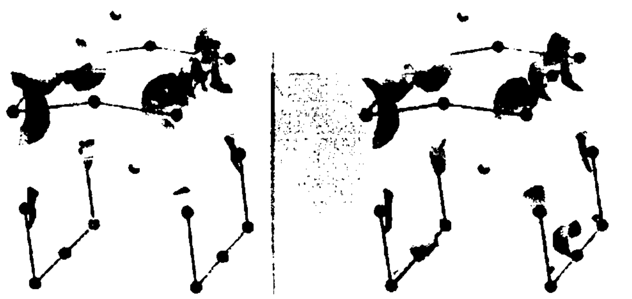

FIG. 3. Wavefunction, squared and symmetrized, of the a–plane band at Y (left) and $\frac{1}{2}\Gamma Y$ (right).

O1(z) becomes allowed and is substantial. The energy increase is, in particular, due to the intra-plane antibonding interaction between O3(z) and Cu2(s) made possible by the dimpling of the plane. As we shall see in the next section (Fig. 5), where we study the adiabatic change of the bands for the Cu2 and O3+O2 Γ_1-modes, decreasing the dimpling decreases the saddlepoint-bifurcation.

Fig. 4 shows the density of states for the individual, hybridized bands in the ±100meV range around ϵ_f. Bands 5 and 4 are the SR-centered hole sticks. Band 3 is essentially the b-band. Band 2 is the a-band with the X-knuckles substituted by part of the chain band, and band 1 is the bulk of the chain band plus the X-knuckles. The van Hove singularities 15 and 25meV below the Fermi level are from the bifurcated Y and X saddlepoints, respectively. The chain-hybridized saddlepoints at U and T are, respectively, 80meV above and 300meV below ϵ_f. Without chain-hybridiztion there would be no $x-y$ asymmetry and no k_z dispersion, all four saddlepoints would therefore coinside and the density-of-states singularity would be logarithmic.

5 ELECTRON-PHONON INTERACTION

In conventional theory the line-width of the νq-phonon due to the e-ph coupling is given by Fermi's golden rule:[17]

$$\gamma_{\nu\mathbf{q}} = 2\pi \sum_{\mathrm{nm}\mathbf{k}} [\theta(\epsilon_{\mathrm{m}\mathbf{k}+\mathbf{q}}) - \theta(\epsilon_{\mathrm{n}\mathbf{k}})]\delta(\epsilon_{\mathrm{m}\mathbf{k}+\mathbf{q}} - \epsilon_{\mathrm{n}\mathbf{k}} - \omega_{\nu\mathbf{q}}) \times |g_{\nu,\mathrm{n}\mathbf{k},\mathrm{m}\mathbf{k}+\mathbf{q}}|^2 \quad (3)$$

Here, $|\mathrm{n}\mathbf{k}\rangle$ are the electronic states in the undistorted

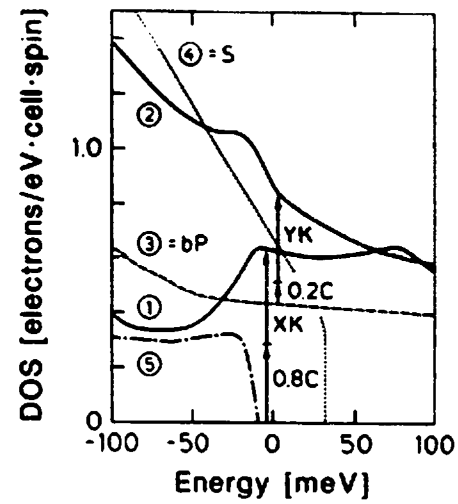

FIG. 4. Density of states for bands 1 to 5, numbered in order of decreasing energy. S denotes the stick, bP the bonding plane band, C the chain band, and XK and YK the X- and Y-knuckles.

crystal, the factor 2 is from the spin-degeneracy, and $\Sigma_{\mathbf{k}} \equiv (2\pi)^{-3} V \int d^3k$ is the average over the Brillouin zone. The e-ph matrix-element is:

$$g_{\nu,\mathrm{n}\mathbf{k},\mathrm{m}\mathbf{k}+\mathbf{q}} = \langle \mathrm{n}\mathbf{k} | \delta V(\mathbf{r}) | \mathrm{m}(\mathbf{k}+\mathbf{q}) \rangle / \delta Q_{\nu\mathbf{q}} \quad (4)$$

with $\delta V(\mathbf{r})$ being the perturbation of the self-consistent electronic potential due to the frozen phonon (2). Now, the Eliashberg function $\alpha^2 F(\omega)$ is essentially the phononic density of states weighted by the relative line-width γ/ω and the strength λ of the e-ph coupling may therefore be expressed as:[17]

$$\lambda \equiv 2\int_0^\infty \frac{\alpha^2 F(\omega)}{\omega} d\omega = \frac{1}{\pi N_\uparrow(0)} \sum_{\nu\mathbf{q}} \frac{\gamma_{\nu\mathbf{q}}}{\omega^2_{\nu\mathbf{q}}} \equiv \sum_{\nu\mathbf{q}} \lambda_{\nu\mathbf{q}}, \quad (5)$$

where $\Sigma_{\mathbf{q}}$ is the average over the Brillouin zone and $N_\uparrow(0) \equiv \Sigma_{\mathrm{n}\mathbf{k}} \delta(\epsilon_{\mathrm{n}\mathbf{k}})$ is the electronic density of states per spin at the Fermi level; according to Fig 4 it is 2.5 states/(eV×$YBa_2Cu_3O_4$×spin).

For the optical, near-Γ_1 phonons ($|\mathbf{q}|$ small, but finite) in 1237, the LDA bands do not give rise to any interband transitions. As $|\mathbf{q}| \equiv$q increases, the first interband transitions are those between the a- and the b-bands, but these are forbidden for the even-parity modes considered here. For small q, the relative phonon line width may then be reduced to the intraband contributions

$$\gamma_{\nu q}/\omega_{\nu 0} = 2\pi \sum_{nk} \delta(\epsilon_{nk})\delta(q\cdot v_{nk}-\omega_{\nu 0})|g_{\nu,nk,nk}|^2, \quad (6)$$

which is a line-integral on the FS. Here, $v_{nk} \equiv \partial\epsilon_{nk}/\partial k$ is

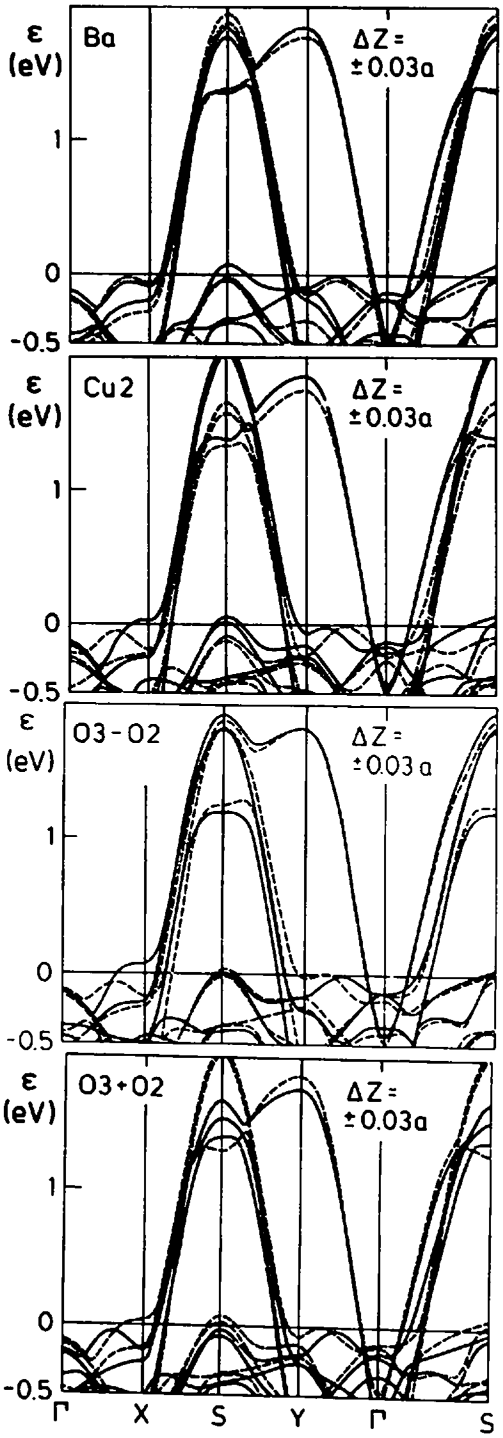

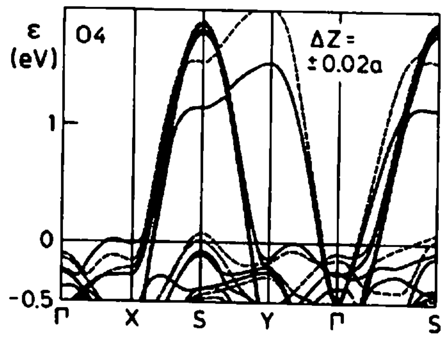

FIG. 5. Selconsistent energy bands for pure Γ_1-mode displacements. Each equivalent atom was displaced by the amount indicated (a=3.83Å). Full (dashed) curves are for positive (negative) displacements (see Table II).

the Fermi velocity and we have linearized the energy bands within the energy range range $\omega_{\nu 0}$ around the Fermi level. Furthermore, we have assumed the existence of a q=0-limit for the e-ph matrix element. This holds when the screening is metallic in all directions, or if we consider transverse modes (q_z=0, in the present case). The intraband e-ph matrix elements (4) are then simply the deformation potentials, i.e., the change of the selfconsistent energy bands relative to the Fermi level $\partial(\epsilon_{nk}-\epsilon_f)/\partial Q_{\nu q}$.

These are shown in Fig. 5 for k_z=0. The Ba_z mode is expected to dipole-shift the chain band with respect to the plane bands. This shift is, however, seen to be tiny, and the largest deformation potential is that of the stick-band. The $Cu2_z$ deformation potential is very similar to that for the $O3_z$+$O2_z$ in-phase dimpling mode, but of opposite sign. The reason is, that the change of the Cu2-O3 and Cu2-O2 hopping integrals dominate. As mentioned in section 4, when the planes (un-) dimple the a-band saddlepoints move away from (towards) X and Y. We see that there is a tendency to pin the Fermi level near the saddlepoint. For the $O3_z$–$O2_z$ mode, there is dimpling in the x-direction and un-dimpling in the y-direction, and vice versa. For this mode, in contrast to the other four modes, the adiabatic Fermi level is not "dragged with the bands" due to the condition of volume conservation for the FS (metallic screening). The deformation potential for the $O3_z$–$O2_z$ mode is therefore stronger than for the $O3_z$+$O2_z$ mode. The $O4_z$ mode has the strongest deformation potential. It mainly shifts the chain bands with respect to the plane bands, not so much due to the dipole shift as due to the modulation of the O4(z)-Cu1(z^2–y^2) hopping integral.

The small-q results for the five Γ_1-phonons (Table II) are shown in Fig. 6 as a function of q. It is obvious that the linewidth is zero for $q < \omega_{\nu 0}/v_{max}$. Had the FS been a cylinder in the z-direction with velocity v, the q-dependence of γ would have been $\theta(x)/\sqrt{x}$, with $x \equiv v^2(q_x^2+q_y^2)-\omega_{\nu 0}^2$. The spikes seen in Fig. 6 thus mark the onsets of the intraband transitions on the various sheets of FS, the ones with lower velocity turn on for larger q. The knuckles are therefore not particularly dominating. The relative linewidths are seen generally to be less than a per cent. The $O2_z$–$O3_z$ and $O4_z$ modes have the largest linewidths. On the right-hand scale of the figure we give the number of phonon-branches (39), times the partial $\lambda_{\nu q}$'s defined in (5). Due to the ω^2 denominator, the relative importance of the the $Cu2_z$ mode increases. An estimate of the total λ may thus be obtained by forming the small-q average for each mode and taking the average over the five modes. The result is $\lambda \approx 0.7$. In the figure we used the pure modes, i.e. e was taken as the unit matrix. With the proper eigenvectors (Table II), we obtain the figure shown in Ref. 7. The main result is, that weight from the large O4 and Cu2 e-ph matrix elements is transferred to, respectively, the 440 and the 110cm^{-1} modes. Since these have lower frequencies, λ increases to 0.8.

The phonon linewidths in Fig. 6 are too small to be observed with neutron scattering. However, additional linewidths and phonon frequency shifts have been observed in Raman scattering ($q \approx 0$) when cooling below T_c.[2] Now, whereas in the normal state the phonon linewidth vanishes for q=0, this is not so for a BCS-like state with a gap. Here, the phonons with frequency $\omega > 2\Delta$ can decay. If we simply pair our LDA electron states around the FS with an empirical gap parameter Δ and then use (3) to calculate the linewidth we obtain[7]

$$\Delta\Sigma_\nu/\omega_\nu \equiv (\Delta\omega_\nu/\omega_\nu) - i(\Delta\gamma_\nu/\omega_\nu) = \lambda_\nu^s f\{\omega_\nu/[2\Delta(T)]\}, \quad (7)$$

dropping the subscript q=0 and with the definition:

$$\lambda_\nu^s \equiv (2/\omega_\nu)\sum_{nk}\delta(\epsilon_{nk})|g_{\nu,nk,nk}|^2. \quad (8)$$

This coupling constant is an average of the deformation potential squared over the entire normal-state FS. The weight-function on the FS is the k-space volume between constant-energy contours such as those seen in the lower part of Fig. 2. It is therefore clear that modes with large deformation potentials at the knuckles will have large λ_ν^s values. This is the case for the O3–O2 mode as seen from our calculated values in Table II. The universal function in (7) is:

$$f(x) \equiv \begin{matrix} -2u/\sin(2u), & \text{for} \quad \sin(u) \equiv x < 1 \\ (2v-i\pi)/\sinh(2v), & \text{for} \quad \cosh(v) \equiv x > 1 \end{matrix}, \quad (9)$$

and we have included the real part of the phonon self-energy Σ. Since eigenvalues repel, it is obvious that phonons with $\omega < 2\Delta$ ($\omega > 2\Delta$) soften (harden) in the superconducting state. Since $f \to -1$ for $\omega << 2\Delta$, low-frequency phonons soften by the relative amount λ_ν^s and, since $Re\, f \to +1$ for $\omega = 2\Delta_+$, a phonon with frequency just above the gap hardens by the relative amount λ_ν^s. This only holds in the weak-coupling BCS limit. In the strong-coupling limit, (7) and (8) are still valid, but the universal function f(x) now depends explicitly on T/T_c and on the impurity scattering time τ. This function which has been evaluated by Zeyher and Zwicknagel[18] exhibits a smearing of the BCS inverse-square-root singularity at $\omega = 2\Delta$, a linewidth broadening also for $\omega < 2\Delta$, and a softening at low ω a bit smaller than λ_ν^s.

Experimental values of λ_ν^s have been obtained for the three uppermost Γ_1-phonons by measuring $\Delta\Sigma/\omega$ as a function of the frequency, fine-tuned by isotope substitution.[14, 15] Fitting to the universal function yields λ_ν^s, Δ, and τ. Since the 330cm^{-1} mode softens and the 440cm^{-1} mode hardens, the gap lies inbetween. The agreement with LDA theory (Table II) is far better than expected.

We now return to the phonon linewidths in the normal state and proceed to finite q. In the small-ω limit, where the energy bands are linear functions of k within the energy range $\omega_{\nu q}$ around the Fermi level and where $q >> \omega_{\nu q}/v_{nk}$, Eq.(3) may be written as a line-integral along the cut between the n'th sheet of the Fermi surface $\epsilon_{nk}=0$ and the m'th sheet of the q–displa-

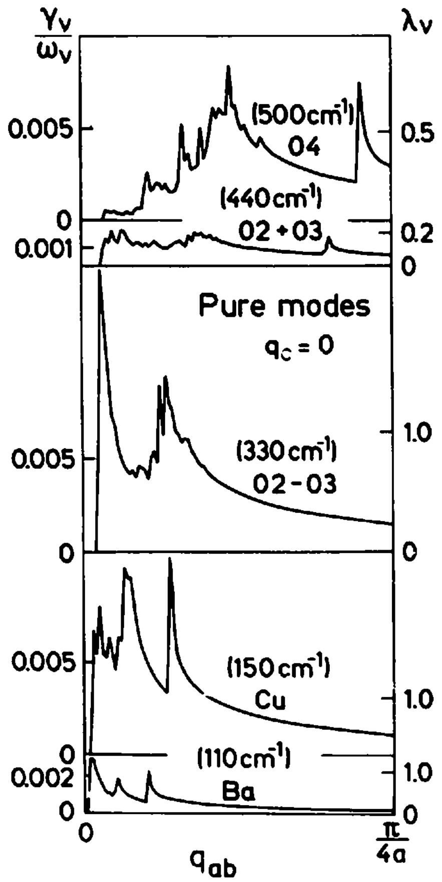

FIG. 6. Calculated intraband contribution to the normal-state relative phonon linewidths, $\gamma_{\nu q}/\omega_{\nu 0}$, and partial coupling constants, $\lambda_{\nu q}$, for the Γ_1-phonons of small, transverse **q**. The average over the directions of **q** in the xy-plane has been taken; $q_{ab} \equiv [q_x^2+q_y^2]^{1/2}$.

ced Fermi surface $\epsilon_{mk+q}=0$:

$$\gamma_{\nu q}/\omega_{\nu q} = 2\pi\sum_{nmk}\delta(\epsilon_{mk+q})\delta(\epsilon_{nk})|g_{\nu,nk,mk+q}|^2 =$$

$$2\pi\sum_{nm}\int\frac{(2\pi)^{-3}V\,dk}{|v_{nk}\times v_{mk+q}|}|g_{\nu,nk,mk+q}|^2 \qquad (10)$$

With muffin-tin orbitals and a frozen-phonon supercell technique, it is inconvenient to evaluate integrals like $\langle nk|\delta V(r)|m(k+q)\rangle$ which involve orbitals at the equilibrium positions and the potential for the displaced atoms. Instead, we obtain the e-ph matrix-elements from the self-consistent energy bands with and without the displacement using that, for a point on the cut, the degeneracy is split by $2|\langle nk|\delta V(r)|m(k+q)\rangle|$.

Our results for γ/ω and the partial λ's for the S_1 and the Y_1-phonons are given in Tables III and IV. Columns labelled "pure" give results calculated assuming e to be the unit matrix. Except for the 50meV S_Γ-mode and the 16meV Y_Γ-mode, the linewidths are still less than one per cent and can hardly be measured. The average λ is 0.7 for the pure S_Γ-modes and it increases (by the previously mentioned mechanism of transferring e-ph coupling to lower-frequency modes) to 1.1 for the properly mixed modes. The average λ for the pure Y_Γ-modes is only 0.7 and, for the mixed modes, we expect it to increase to about 1. In conclusion, summing over all 17 modes considered, we find:

$$\lambda \approx 1.0, \qquad (11)$$

which seems to rule out the e–ph interaction as the *sole* mechanism for the high-temperature superconductivity.

7 *Im* $\chi^0(q,\omega)$.

For **q**=**S**, the important contributions to (10) are the transitions from the X knuckle to the Y knuckle. For **q**=**Y**, the important contributions are the transitions between the stick and the X knuckle, and between the Y_+ and the Y_- knuckles. One may now ask whether there would be special values of **q** where for phase-space reasons, like nesting, the linewidth could be large. For this purpose we have calculated

$$\gamma(q,\omega) \equiv 2\pi g^2\sum_{nmk}[\theta(\epsilon_{mk+q})-\theta(\epsilon_{nk})]\delta(\epsilon_{mk+q}-\epsilon_{nk}-\omega_{\nu q})$$

$$= -2g^2\, Im\, \chi^0(q,\omega)\,. \qquad (12)$$

For small ω we used (10). The constant matrix element, g, was chosen such that $\gamma(q,\omega)/\omega$ reproduces the value $\gamma/\omega = 1.5\%$ for the pure breathing mode at S (Table III). Hence, g = 28meV. The result is shown in Fig. 7. The two large peaks present for small ω near $q={}^2/_3\Gamma Y$ and $^1/_2\Gamma X$ are due to the nesting of the Y_- and Y_+ knuckles and of the X_- and X_+ knuckles, respectively. This nesting is illustrated in the upper part of Fig. 2. The "mountain-ridge" running across the Brillouin zone from X to Y is caused by the stick to a-band transitions. Conventional nesting between the flat parts of the a-

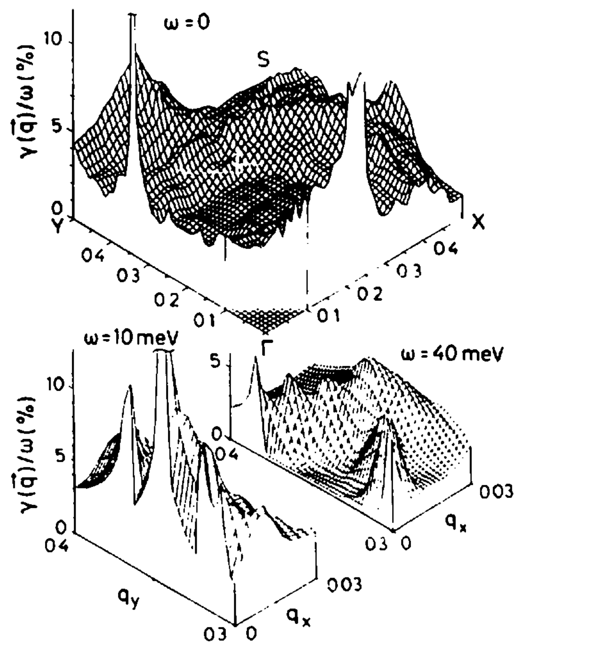

FIG. 7. $\gamma(\mathbf{q},\omega)/\omega$ as given by (12) for $q_z=0$. The trivial singularity at Γ has been cut away. For $\omega=10$ and 40meV only the q–space region around $^2/_3\Gamma Y$ is shown.

band sheet has $\mathbf{q} \approx 0.6\Gamma S$, as seen in the upper left part of Fig. 2. Conventional nesting gives a relatively small contribution to $\gamma(\mathbf{q},\omega)$ due to the high velocities on these parts of the Fermi surface.

Since the saddlepoints are merely 15 and 25meV below the Fermi level the ω-dependence of the peaks in $Im\,\chi^0(\mathbf{q},\omega)/\omega$ should be strong and this is indeed the case as seen in the lower part of Fig. 7. For ω exceeding the saddlepoint energy, the situation is like for q=0 (Fig. 6): Transitions can only take place for $|\mathbf{q}-\mathbf{q}_0| > \omega/v$. Here, again we might expect additional linewidths to develop in the superconducting state.

It is interesting that it is in the q–space regions around $^2/_3\Gamma Y$ and $^1/_2\Gamma X$ that an "extra branch" or an anomalously large phonon broadening was observed by neutron scattering.[9] Also, dynamical superstructures observed in the Tl-compounds[3] may be due to such "saddle-point nesting".

We have finally investigated whether saddlepoints near ϵ_f could be a reason for the quasi-electron linewidth $Im\,\Sigma(\mathbf{q},\epsilon_q)$ to increase more like $|\epsilon_q-\epsilon_f|$ than like $(\epsilon_q-\epsilon_f)^2$, as is the case for a normal Fermi liquid. For a two-dimensional electron gas with a saddlepoint at ϵ_f we have calculated the response function $\chi^0(\mathbf{q},\omega)$ and $Im\,\Sigma(\mathbf{q},\epsilon_q)$ analytically. We find that $Im\,\chi^0(\mathbf{q},\omega)$ is constant down to arbitrary small ω for certain directions of q. As a result, $Im\,\Sigma(\mathbf{q},\epsilon_q) \propto (\epsilon_q-\epsilon_f)^{3/2}$, and thus grows faster than $(\epsilon_q-\epsilon_f)^2$ although not as fast as $|\epsilon_q-\epsilon_f|$. For the saddlepoint being ω_0 from ϵ_f, this behaviour holds for $|\epsilon_q-\epsilon_f| \gtrsim \omega_0$. Our model differs from the one of Virosztek and Ruvalds,[10] who relied on nesting of flat FS-parts. It is similar to the model of Newns et al. who, however, introduced additional approximations and obtained a different analytical form.

REFERENCES

1J.C. Campuzano et al., Phys. Rev. **B43** (1991) 2788; B.O. Wells et al., Phys. Rev. Lett. **65** (1990) 3056; G. Mante et al., Z. Phys. **B80** (1990) 181.

2C. Thomsen and M. Cardona in: Physical Properties of High-Temperature Superconductors, ed. D.M. Ginsberg (World Scientific, Singapore, 1989) 409

3B.H. Toby et al., Phys. Rev. Lett. **64** (1990) 2414; H.A. Mook et al. ibid **65** (1990) 2712

4Review: W. Pickett, Rev. Mod. Phys. **61** (1989) 433.

5S. Gopalan et al., this volume.

6E.T Heyen et al., Phys. Rev. Lett. **65** (1990) 3048.

7C.O. Rodriguez et al., Phys. Rev. **B42** (1990) 2692; C. Thomsen et al., Solid State Commun. **75** (1990) 219.

8R.E. Cohen et al., Phys. Rev. Lett. **64** (1990) 2575; W.E. Pickett et al., Phys. Rev. **B42** (1990) 8764.

9W. Reichardt et al., Physica **C 162–164** (1989) 464; L. Pintschovius, this volume.

10A. Virosztek and J. Ruvalds, Phys. Rev. **B42** (1990) 4064; D.M. Newns et al., Phys. Rev. **B43** (1991) 3075.

11M. Methfessel, C.O. Rodriguez, and O.K. Andersen, Phys. Rev. **B40** (1989) 2009.

12A. Simon et al., J. Solid. State Chem. **77** (1988) 200.

13M.A. Beno et al., Appl. Phys. Lett. **51** (1987) 57

14B. Friedl et al. Phys. Rev. Lett. **65** (1990) 915.

15B. Friedl et al. Sol. State Commun. **76** (1990) 1107.

16C.M. Fowler et al. Phys. Rev. Lett. (submitted).

17P.B.Allen, Phys. Rev. **B6** (1972) 2577.

18R.Zeyher and G.Zwicknagl Z. Phys. **B78** (1990) 175.